UNSTEADY CHARACTERISTICS OF LIFT GENERATED BY SMALL UNDERWATER CONTROL FIN

(DOI No: 10.3940/rina.ijme.2016.a4.348)

M Yoshida, Kyushu University, Japan, **H Iwashita**, Hiroshima University, Japan, **M Kanda**, Mitsui Engineering & Shipbuilding Co., Ltd., Japan, **H Kihara**, National Defense Academy of Japan, Japan and **T Kinoshita**, The University of Tokyo, Japan

SUMMARY

Speed reduction or slamming must be restricted for a high-speed oceangoing vessel because of the requirement for punctuality and the high value of the cargo. Speed reduction and slamming are caused by large amplitude motions in waves. A promising ship form for such vessels is so-called "Resonance-Free SWATH (RFS)", which has negative pitch and roll restoring moments due to the extraordinary small water plane area. As a consequence, the resonance peak is removed from the motion response. The attitude of the RFS with negative restoring moments is adjusted by four pairs of control fins attached to the fore and aft ends of the lower hulls. In previous studies, the steady value of the lift-curve slope is usually used in the motion equation of the frequency domain. However, when working in waves, the controlling fins are not working in a steady state and the lift coefficient is no longer a constant. In addition, there exists a phase lag between the change in the attack angle and the fin-generated lift. In the present study, theoretical predictions using a frequency-domain 3D-Rankine Panel Method, as well as experimental measurement, have been made to analyze the phenomena of the lift generation including the phase lag and the interference between fins, the lower hulls and the struts. The theoretical results agree well with the experimental results in spite of the potential theory being without viscosity. Next, the unsteady characteristics of fin-generated lift are expressed as the function of the encountering wave frequency. Then the effects of the fore fins, the lower hulls and struts on the lift curve-slope of the aft fins are discussed.

NOMENCLATURE

A	Plane area of fin (m^2)
A_w	Water plane area (m^2)
α_{cj}	Attack angle of fin control (rad)
B	Breadth of ship (m)
c	Chord length (m)
$C_{L\alpha}$	Lift-curve slope for attack angle (rad^{-1})
d	Draught (m)
F_n	Froude number (-)
g	Acceleration of gravity (m s^{-2})
GM_L	Longitudinal metacentric height (m)
K	Wave number (m^{-1})
L	Length of ship (m)
ℓ_0	Moment lever of fin (m)
R_e	Reynolds number (-)
ρ	Density of water (kg m^{-3})
U	Ship speed (m s^{-1})
V	Displaced volume (m^3)
ω_0	Wave frequency (s^{-1})
ω_e	Encountering frequency (s^{-1})
ξ_j	Displacement in j-th motion (m/rad)
ζ_a	Amplitude of incident wave (m)

1. INTRODUCTION

Research and development on the seaworthiness of oceangoing ships has been pursued actively before [1], [2], [3]. In some works, the effect of control fins on the motion responses has been studied. However steady state values have been used as an approximation for the fin-generated lift [4], [5], [6], and the unsteady effects on the fin-generated lift have not been considered in most of the studies. When the control of ship motions by means of the fins is considered, the unsteady characteristics such as the time lag and the interaction between fins and the hulls are very important [7], [8], [9], [10], since they have a profound effect on the magnitude of the maximum control gain, the lift force itself and the consequent motion responses.

A promising ship form for a fast oceangoing vessel is the so-called "Resonance-Free SWATH (RFS) [11], [12]", whose motion is reduced completely even in rough seas. It has negative restoring moments due to its extraordinary small water plane area. The attitude of the RFS is adjusted by four pairs of control fins attached to the fore and aft ends of the lower hulls. As a result, the motion responses of the RFS [12] are significantly reduced compared with those of the mono-hull and the trimaran.

In the present study, some calculated and experimental results for the hydrodynamic forces and moments acting on the fins attached to the RFS, especially the unsteady characteristics of fin-generated lift, are presented and discussed.

2. THEORETICAL CALCULATIONS

2.1 MATHEMATICAL FORMULATION

In the present study, a three dimensional frequency-domain Rankine Panel Method (3D-RPM) based on the potential theory [13], [14] has been applied to calculate the hydrodynamic forces and moments. The calculations have been carried out for the RFS model shown in Figure 1. The RFS model consists of an upper deck, two struts and twin lower hulls. The cross section of the lower hulls is circular with a maximum diameter of 0.077 m. The horizontal cross section of the strut is elliptical with a length of 0.783 m and a maximum breadth of 0.0385 m. The height of the strut is approximately 0.154 m. Four pairs of horizontal control fins and two pairs of vertical rudders are attached to the lower hulls. Each fin has the following configuration: Plane area A = 0.001518 m^2, chord length c = 0.0357 m (base) or 0.0278 m (tip), span s = 0.0478 m, aspect ratio s^2/A=1.51 and the symmetrical wing profile of NACA0012.

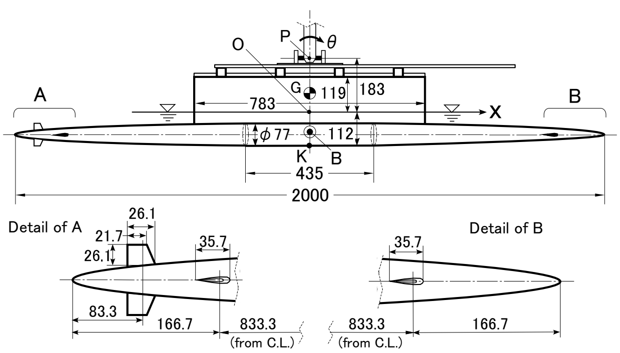

(a) Side view (unit: mm)

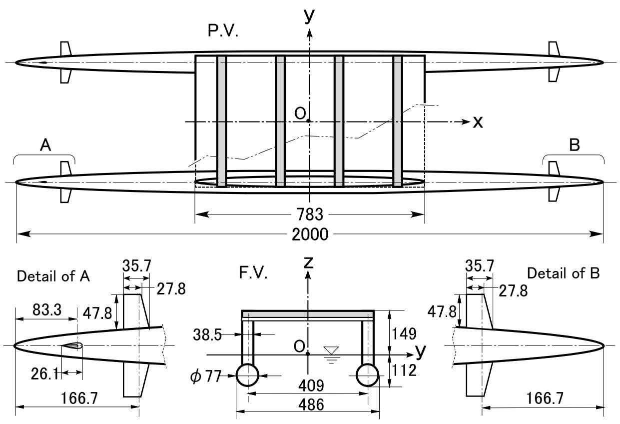

(b) Plane and front view (unit: mm)

Figure 1: Plan of RFS model indicating condition for calculations

a) Boundary conditions

The fluid is assumed to be ideal and the flow irrotational. When the ship is advancing at a constant forward speed U in oblique regular waves encountered at an angle of χ, the velocity potential Φ , governed by Laplace's equation, can be expressed as

$$\Phi(x,y,z;t) = U[-x + \phi_s(x,y,z)] + \mathrm{Re}[\phi(x,y,z)e^{i\omega_e t}] \quad (1)$$

Where

$$\phi = \frac{g\zeta_a}{\omega_0}(\phi_0 + \phi_7) + i\omega_e \sum_{j=1}^{6} \xi_j \phi_j \quad (2)$$

$$\phi_0 = ie^{Kz - iK(x\cos\chi + y\sin\chi)} \quad (3)$$

$$\omega_e = \omega_0 - KU\cos\chi \quad (4)$$

ζ_a , ω_0 and K indicate the amplitude, the angular frequency and the wave number of the incident wave respectively. ω_e denotes the encountering frequency and g the gravitational acceleration. The potential ϕ_s represents the steady wave field, and ϕ_j the unsteady wave field. For the steady potential ϕ_s , the following boundary conditions at the free surface S_F , the body surface S_H and the wake sheets S_W of the fins are satisfied.

$$U^2 \frac{\partial^2 \phi_s}{\partial x^2} + g\frac{\partial \phi_s}{\partial z} = 0 \qquad \text{on } z=0 \quad (5)$$

$$\frac{\partial \phi_s}{\partial n} = n_1 \qquad \text{on } S_H \quad (6)$$

$$\Delta P = P^+ - P^- = 0 \qquad \text{on } S_W \quad (7)$$

Where $\vec{n}$ is the unit normal vector on the body surface pointing into the fluid. The Kutta condition, that the pressure difference $\Delta P = P^+ - P^-$ between the upside and downside of the wake sheet leading out of the trailing edge of the underwater fin is equal to zero, is described in Equation (7). On the other hand, for the unsteady potential ϕ_j , the following boundary conditions are satisfied.

$$-\omega_e^2 \phi_j - i2U\omega_e \frac{\partial \phi_j}{\partial x} + U^2 \frac{\partial^2 \phi_j}{\partial x^2} + g\frac{\partial \phi_j}{\partial z} = 0 \qquad \text{on } z=0 \quad (8)$$

$$\left.\begin{aligned} \frac{\partial \phi_j}{\partial n} &= n_j + \frac{U}{i\omega_e} m_j \ (j = 1-6) \\ \frac{\partial \phi_7}{\partial n} &= -\frac{\partial \phi_0}{\partial n} \end{aligned}\right\} \qquad \text{on } S_H \quad (9)$$

$$\Delta P = P^+ - P^- = 0 \qquad \text{on } S_W \quad (10)$$

The normal vectors are defined as follows:

$$(n_1, n_2, n_3) = \vec{n}, \ (n_4, n_5, n_6) = \vec{r} \times \vec{n} \quad (11)$$

$$(m_1, m_2, m_3) = -(\vec{n}\cdot\nabla)\vec{V}, \ (m_4, m_5, m_6) = -(\vec{n}\cdot\nabla)(\vec{r}\times\vec{V}) \quad (12)$$

with $\vec{r} = (x,y,z), \ \vec{V} = \nabla(-x + \phi_s)$

Where, the so-called m-term, i.e. m_j in Equation (9) or Equation (12), is an influence term from the steady flow to the unsteady flow on the body surface. That is, it represents the effect of the forward speed on the unsteady flow. Assuming that the influence of the steady disturbance potential ϕ_s is small, the m-term is simplified to:

$$(m_1, m_2, m_3) = (0,0,0), (m_4, m_5, m_6) = (0, n_3, -n_2) \quad (13)$$

In addition, the infinite water depth condition and the radiation condition at the infinitely far field are satisfied by ϕ_s and ϕ_j .

b) Hydrodynamic forces and lift forces

The pressure in the unsteady flow

$$P(x, y, z; t) = \mathrm{Re}[p(x, y, z)\, e^{i\omega_e t}] \quad (14)$$

is obtained by the Bernoulli's pressure equation as follows.

$$p(x, y, z) = -\rho\,(i\omega_e - U\frac{\partial}{\partial x})\phi \quad (15)$$

By integrating the pressure over the hull surface, the unsteady hydrodynamic forces and moments F_i are evaluated as follows.

$$F_i = -\iint_{S_H} p(x, y, z)\, n_i\, dS,\ \ (i = 1-6) \quad (16)$$

In the present study, the effect of the incident waves is not taken into account. The ship hull is advancing at a uniform speed in still water. Hence, the hull has no oscillation and only the fin rotates around its axis back and forth. Accordingly, the diffraction problem is not solved and only the radiation problem is discussed now. The boundary condition at the body surface of Equation (9) is rewritten as follows.

$$\frac{\partial \phi_5}{\partial n} = 0 \quad \text{on } S_H \text{ except for fin surface} \quad (17)$$

$$\frac{\partial \phi_5}{\partial n} = n_5' + \frac{U}{i\omega_e} m_5' = n_5' + \frac{U}{i\omega_e} n_3 \quad \text{on fin surface} \quad (18)$$

Here $\vec{n}'$ represents the unit normal vector which is transformed into the local coordinate system with its origin at the rotating axis of the fin. Then, the hydrodynamic forces and moments produced by the pitch motion of the fin around its axis are calculated as follows.

$$\frac{F_i}{\xi_5} = -\rho\omega_e^2 \iint_{S_H} \left(\phi_5 - \frac{U}{i\omega_e} \frac{\partial \phi_5}{\partial x} \right) n_i\, dS,\ \ (i = 1, 3, 5) \quad (19)$$

Accordingly, the fin-generated lift force is calculated as follows.

$$L_f = \frac{1}{2}\left(F_3 - \frac{F_5 + F_1 l_0}{x_f} \right)$$
$$L_a = \frac{1}{2}\left(F_3 - \frac{F_5 + F_1 l_0}{x_a} \right) \quad (20)$$

Here L_f or L_a indicates the lift generated by the fore or aft fin, centred at (x_f, y_f, z_f) or (x_a, y_a, z_a) respectively referring to the global system, and $l_0 \approx |z_f| = |z_a|$.

c) The Kutta condition

According to the method of approximation developed by Morino and Kuo [15], the pressure difference between the upperside and underside of the wake sheet S_W in the unsteady problem is expressed by the following equation.

$$\Delta P = -\rho(i\omega_e - U\frac{\partial}{\partial x})\,\Delta\phi_j(x, y, z) = 0 \quad \text{on } S_W \quad (21)$$

Here, $\Delta\phi_j$ denotes the potential difference between the two sides of the wake sheet, which is assumed to take the following form:

$$\Delta\phi_j(x, y, z) = A(y, z)\, e^{ikx} \quad (22)$$

Substituting Equation (22) into the Kutta condition given in Equation (21), it is easy to obtain:

$$k = \frac{\omega_e}{U} \quad (23)$$

Equation (22) will hold at the trailing edge of the fins located at (x_T, y_T, z_T) as well, i.e.

$$\Delta\phi_j(x_T, y_T, z_T) = \phi_{jT}^+ - \phi_{jT}^- = A(y_T, z_T)\, e^{ikx_T} \quad (24)$$

Accordingly,

$$A(y_T, z_T) = (\phi_{jT}^+ - \phi_{jT}^-)\, e^{-ikx_T} \quad (25)$$

Where the value of the velocity potential at the upperside and underside of the trailing edge is written as ϕ_{jT}^+ and ϕ_{jT}^- respectively. It is assumed that the value of $A(y, z)$

is unchanged in the wake after leaving the trailing edge of the fins. Equation (22) is now simplified as:

$$\Delta\phi_j(x, y_T, z_T) = (\phi_{jT}^{+} - \phi_{jT}^{-})\, e^{ik(x-x_T)} \tag{26}$$

In the case of the steady problem, k in Equation (26) is equal to zero apparently.

2.2 NUMERICAL METHODS

Boundary value problems given in Equations (5)–(7) and (8)–(10) are solved by using the boundary element method respectively. In the case of unsteady problem, the integral equation is derived as follows:

$$\begin{aligned}
&\frac{\phi_j(P)}{2} - \iint_{S_H} \frac{\partial G(P,Q)}{\partial n} \phi_j(Q) dS \\
&\quad + \iint_{S_F} \left[\frac{\partial \phi_j(Q)}{\partial n} - \phi_j(Q) \frac{\partial}{\partial n} \right] G(P,Q) dS \\
&\quad - \iint_{S_W} \frac{\partial G(P,Q)}{\partial n} \Delta\phi_j(Q) dS \\
&\quad = - \iint_{S_H} \frac{\partial \phi_j(Q)}{\partial n} G(P,Q) dS
\end{aligned} \tag{27}$$

Where

$$P = (x, y, z),\; Q = (x', y', z') \tag{28}$$

$$G(P,Q) = \frac{1}{4\pi r},\; r = |P - Q| \tag{29}$$

The following expression is obtained from Equation (26).

$$\Delta\phi_j(Q) = (\phi_{jT}^{+} - \phi_{jT}^{-})\, e^{ik(x'-x_T)} \tag{30}$$

The velocity potentials $\phi_j(Q)$ on the free surface, the hull surface and the fin surface are unknowns in the integral equation (27). In the present study, the spline finite element method developed by Sclavounos and Nakos [16] is adopted to evaluate the integral over the free-surface. That is, the velocity potential ϕ_j on the free-surface z=0 is described as follows.

$$\phi_j(x, y) = \sum_{m=1}^{N_F} \lambda_m B_m(x, y) \tag{31}$$

Here $B_m(x, y)$ is the two-dimensional cubic B-spline function, λ_m the spline coefficients and N_F the number of panels on the free-surface. Then, the free-surface condition is expressed as follows.

$$\frac{\partial \phi_j}{\partial n} = -\frac{\partial \phi_j}{\partial z} = \sum_{m=1}^{N_F} \lambda_m \sum_{k=0}^{2} C_k \frac{\partial^k}{\partial x^k} B_m(x, y) \tag{32}$$

Where

$$C_0 = -K_e,\; C_1 = -i2\tau,\; C_2 = \frac{1}{K_0} \tag{33}$$

$$K_e = \frac{\omega_e^2}{g},\; \tau = \frac{U\omega_e}{g},\; K_0 = \frac{g}{U^2} \tag{34}$$

Assuming that the surfaces S_F, S_H or S_W consists of N_F, N_H or N_W panels respectively and the value of the velocity potential is constant in each panel, the integral equation (26) is discretized as follows.

$$\begin{aligned}
&\frac{\phi_j^*(k)}{2} - \sum_{l=1}^{N_H} \left[\phi_j^*(l)\, G_n^*(k,l) + \delta\phi_j^*(l) \sum_{n=1}^{N_W} G^*(k,n)\, e^{ik(x_n - x_T)} \right] \\
&- \sum_{m=N_H+1}^{N_H+N_F} \lambda_{m-N_H} \\
&\quad \times \sum_{l=N_H+1}^{N_H+N_F} \left[G_n^*(k,l)\, B_{m-N_H} - G^*(k,l) \sum_{k=0}^{2} C_k \frac{\partial^k}{\partial x^k} B_{m-N_H} \right] \\
&= -\sum_{l=1}^{N_H} \frac{\partial \phi_j^*(l)}{\partial n} G^*(k,l)
\end{aligned} \tag{35}$$

Where $\phi_j^*(k)$ indicates the value of the velocity potential ϕ_j of k-th panel and

$$\begin{Bmatrix} G^*(k,l) \\ G_n^*(k,l) \end{Bmatrix} = \iint_{\Delta S(l)} \begin{Bmatrix} G(P_k, Q) \\ \dfrac{\partial G(P_k, Q)}{\partial n} \end{Bmatrix} dS \tag{36}$$

Here P_k denotes the representative position of the k-th panel and $\Delta S(l)$ the area of the l-th panel. Also, δ is non-trivial only in the case that l lies on the panel next to the trailing edge, and then l is equal to +1 on the top surface panel, -1 on the under surface panel. Finally, Equation (35) becomes a system of the simultaneous algebraic equations, in which ϕ_j^* and λ_m are regarded as unknowns.

For the purpose of reference, the computation grids adopted in the present study are shown in Figure 2. The panels on the bodies including the struts, lower hulls and fins are in red, while the panels on the free surface are in blue, as illustrated in Figure 2 (a). The panels on the wake sheets are shown in Figure 2 (b). In the figure, the panels on the wake sheets of fore fins are in blue, while the panels on the wake sheets of aft fins are in green.

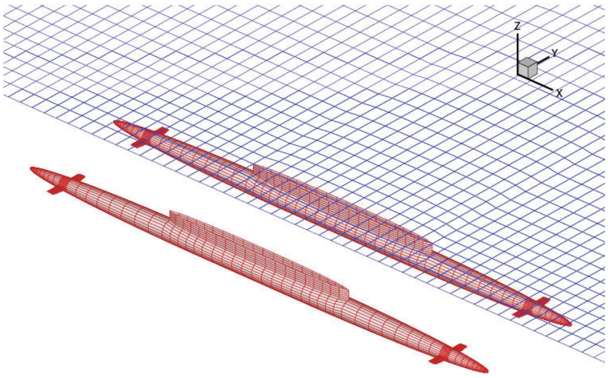

(a) Grids on ship hull, fins and free surface

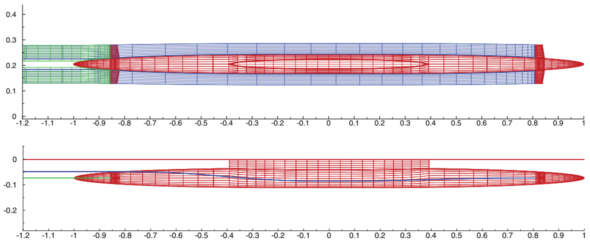

(b) Grids on wake sheets of fore and aft fins

Figure 2: Computation grids applied in calculations

3. EXPERIMENTS

3.1 MODEL AND MODEL BASINS

In a previous study [12], experiments were carried out to measure the lift forces acting on the fore and aft fins of the RFS model. A photograph of the RFS model is shown in Figure 3. The principal particulars of the model are presented in Table 1. The scale size of the model is equal to 1/115. Since the longitudinal metacentric height GM_L is equal to −0.019 m, the model has negative pitch restoring moment.

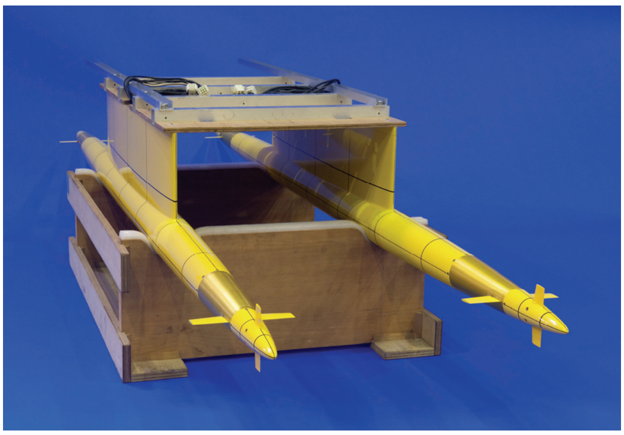

Figure 3: Overview of RFS model [12]

The experiments were carried out at the Ocean Engineering Basin in The University of Tokyo and Small Towing Tank of Akishima Laboratories (Mitsui Zosen) Inc.

Table 1: Principal particulars of RFS model

Scale size	L_{model}/L_{real}	1/115
Length	L (m)	2.0
Breadth	B (m)	0.486
Draught	d (m)	0.112
Water plane area	A_w (m^2)	0.0473
Height of gravity center	KG (m)	0.180
Longitudinal metacentric height	GM_L (m)	−0.019
Radius of gyration	κ_{yy}/L	0.207
Mass	ρV (kg)	15.49
Advancing speed	U (m/s)	1.918
Froude number	F_n	0.433
Reynolds number (hull)	R_{e_hull}	4×10^6
Reynolds number (fin)	R_{e_fin}	6×10^4

3.2 CONTROLLING THE FINS

Four sets of fin controlling equipment are installed in the bow and stern of both lower hulls, where the diameter of the lower hull is about 40 mm. The controlling equipment consists principally of a DC servomotor, worm gear, fin axis and potentiometer. The attack angle of the four pairs of movable fin equipment can be controlled independently. The maximum amplitude of attack angle of each fin is limited to 20 deg, and the maximum frequency of fin oscillation is 3.0 Hz.

3.3 EXPERIMENTAL CONDITIONS

The tests for measuring the fin-generated lift were carried out at an advancing speed of U=1.918 m/s (F_n= 0.433) in still water. During the experiment, the motion of the hull is fixed, and the fore and aft fins are forced to rotate sinusoidally around their axes. The range of oscillation frequency ω is 0-19 rad/s and the rotating amplitude of oscillation is 10 deg. Four oscillation modes of fins have been tested as shown in Figure 4. When controlling the heave motion, both fore and aft fins rotate in the same phase, whilst when controlling the pitch motion, they rotate in the opposite phase.

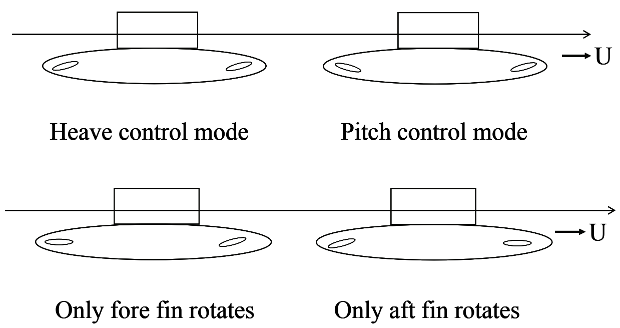

Figure 4: Four oscillation modes of fins tested to find out unsteady characteristics of lift

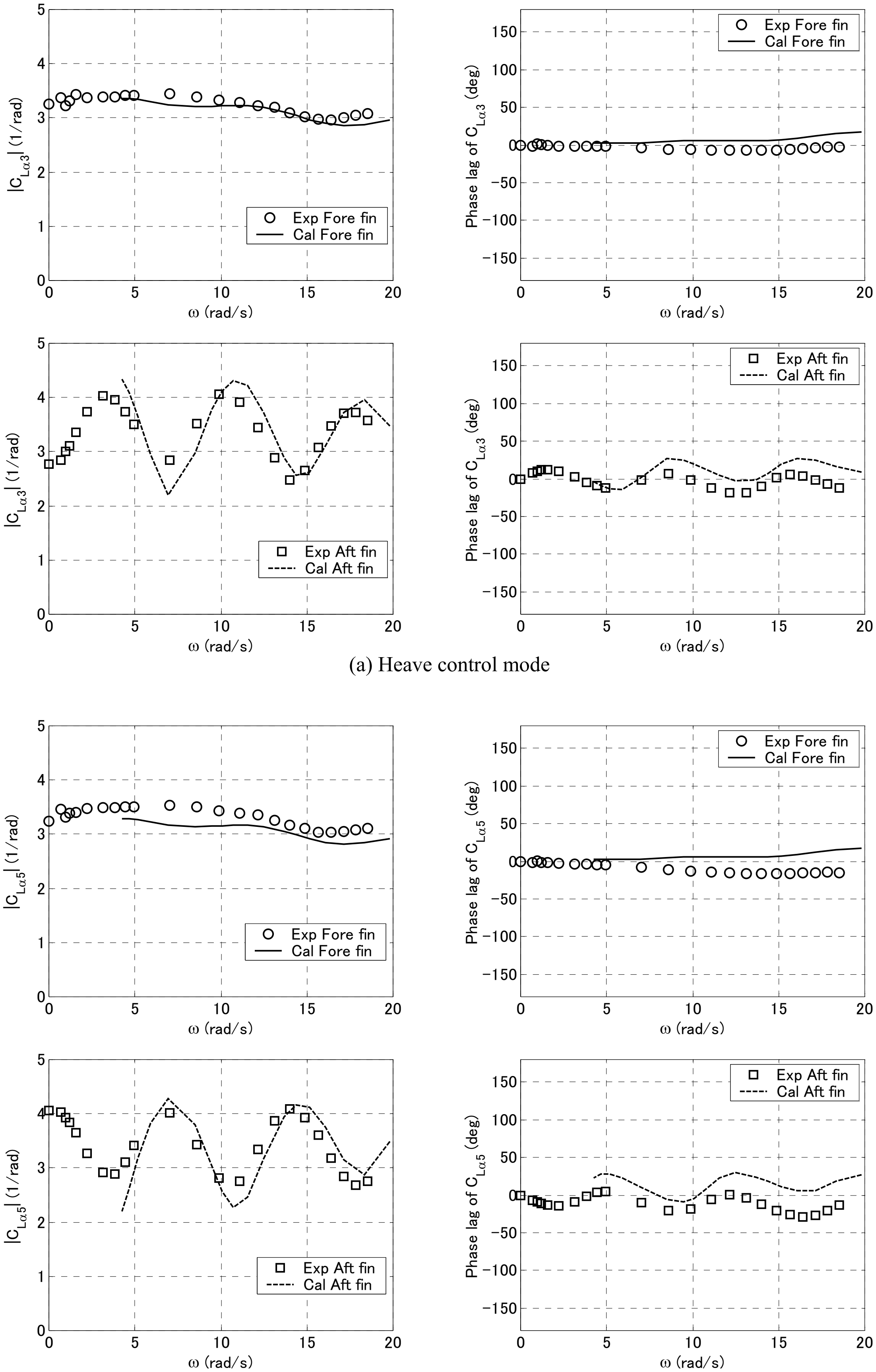

(a) Heave control mode

(b) Pitch control mode

Figure 5: Unsteady characteristics of lift acting on fore or aft fin (effect of oscillation frequency of fin on lift-curve slope and phase lag)

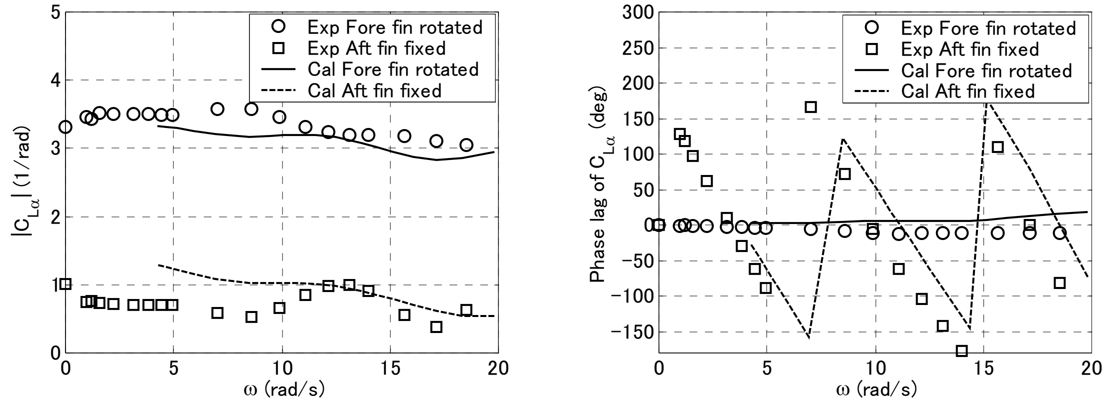

(a) Fore fin rotated and aft fin fixed

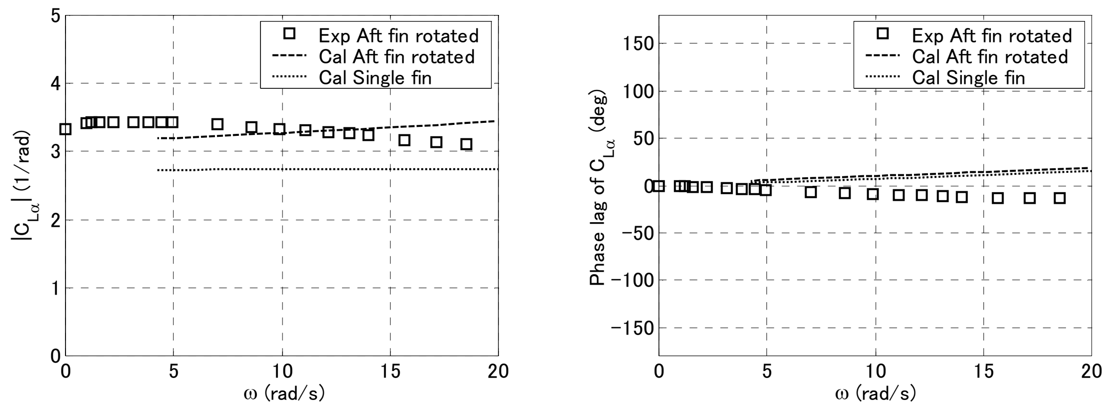

(b) Fore fin fixed and aft fin rotated

Figure 6. Unsteady characteristics of lift in the case that only fore or aft fin operates alone (effect of oscillation frequency of fin on lift-curve slope and phase lag)

In the 3rd or 4th mode, only the fore or aft fin is rotated and the angle of the aft or fore fin is fixed at zero degrees relative to the longitudinal hull axis.

Also, visualization tests of the flow around the lower hull has been carried out using a model in which small tufts are attached to the lower hull of the model advancing at F_n=0.433 in still water as shown later in Figure 7.

4. RESULTS AND DISCUSSIONS

4.1 UNSTEADY CHARACTERISTICS OF FIN-GENERATED LIFT

Calculated and experimental measurements of the fin-generated lift for the RFS model are presented in Figure 5 and Figure 6. In Figure 5 $C_{L\alpha 3}$ indicates the lift-curve slope with respect to the attack angle operating in the heave control mode, while $C_{L\alpha 5}$ denotes that in the pitch control mode. In Figure 6, $C_{L\alpha}$ represents the lift-curve slope of the fins in the case where the fore or aft fin rotates alone. The unsteady characteristics of the fin-generated lift such as the time lag of lift-generation (i.e. the phase lag) and the interaction between the fore fins, the aft fins, the struts and the lower hulls are shown in these figures.

Next, calculations have been carried out for the condition where the wake sheet of the fore fin passes above the aft fin with a height of 25 mm. These are confirmed by the experimental visualization test of the flow around the lower hull as shown in Figure 7. The photographs shown in Figure 8 demonstrate the average flow passing over the surface of the aft fin during the oscillation of the fin for the case of the heave control mode at ω=7.0 rad/s (Figure 8 (a)) and the case of the pitch control mode at ω=11.1 rad/s (Figure 8 (b)). The flow goes down from the fore fin to the midship bottom, and then goes up and passes above the aft fin for every oscillation frequency in both modes.

It can be seen that:

Firstly, the theoretical results agree well with the experimental results, especially in the case of the amplitude of the lift-curve slope, in spite of the potential theory being without the viscosity.

Secondly, as a whole, the amplitude of the lift-curve slope gets smaller slightly and the phase lag becomes larger slightly as the frequency ω increases, according to the experimental results. This is the feature, which is generally as predicted. Accordingly, the maximum value of the control gain is limited by the presence of the time lag, and then the effect of the motion control using the fin-generated lift consequently becomes restricted as shown in previous studies [17], [18].

Thirdly, considering Figure 5 in detail, it is understood that the amplitude of the lift-curve slope of the aft fin has a periodic fluctuation i.e. hump and hollow in both the heave and pitch control modes, while there exists no hump and hollow for that of the fore fin. Also, as regarding the phase lag, there seems to be the same feature. In other words, the lift-generation of the aft fin is affected by the wake sheet of the fore fin in general. Furthermore, regarding the hump and hollow of the periodic fluctuation with respect to the frequency ω, there seems to be the opposite feature in the amplitude and the phase lag of the lift-curve slope when comparing the control modes of heave and pitch. This phenomenon is confirmed from Figure 6 (b), which shows that the lift generated by the aft fin has no fluctuation with respect to the frequency when only the aft fin rotates. It means that the fixed fore fin does not affect the amplitude or the phase lag of the lift generated by the aft fin. Also, Figure 6 (a) shows the results in the case that only the fore fin is rotated and the aft fin is fixed. The amplitude and the phase lag of the lift generated by the fore fin indicate the same feature as those in the heave or pitch control mode in Figure 5. On the other hand, the amplitude or the phase lag of the fixed aft fin shows the value which is more than zero. This is caused by the effect of the wake sheet of the fore fin. Namely, the aft fin fixed at zero angle has relative attack angle due to the wake sheet of the fore fin.

Finally, calculations have also been carried out for the condition that the single fin rotates around its axis beneath the free surface. In this case, the interaction between the fins, struts and lower hulls is not considered. The results are presented in Figure 6 (b). The calculated magnitude of the lift amplitude is smaller than that of the experimental results using the model, while the phase lags of both results agree roughly. The reason for the difference in amplitude is the existence of the hull.

4.2 INTERFERENCE BETWEEN BODY AND FIN

Now considering the lift-curve slope with respect to the attack angle in the steady state, it is expressed as

$$C_{L\alpha} = (k_{W(B)} + k_{B(W)})(C_{L\alpha})_W \tag{37}$$

based on the aerodynamic study of body-fin interference by Pitts et al. [19], where

$$k_{W(B)} = \frac{(C_{L\alpha})_{W(B)}}{(C_{L\alpha})_W},\quad k_{B(W)} = \frac{(C_{L\alpha})_{B(W)}}{(C_{L\alpha})_W} \tag{38}$$

Here the subscript W represents the case of the fin alone, $B(W)$ the case of the lift on the body induced by the fin, and $W(B)$ the case of the lift on the fin induced by the body. For low aspect ratio fins, $(C_{L\alpha})_W$ is evaluated using a formula proposed by Whicker and Fahlner [20] such as

$$(C_{L\alpha})_W = \frac{1.8\pi A_e}{1.8 + \sqrt{A_e^2 + 4}} \quad \text{per radian} \tag{39}$$

and

$$A_e = (r_0 - \frac{r^2}{r_0})/c \tag{40}$$

where A_e is the effective aspect ratio, r indicates the radius of the body, r_0 denotes the transverse distance from the body axis to the tip of the fin and c represents the average chord length of the fin. In the present study, it is obtained that A_e = 2.0 and then $(C_{L\alpha})_W$ = 2.44 1/rad.

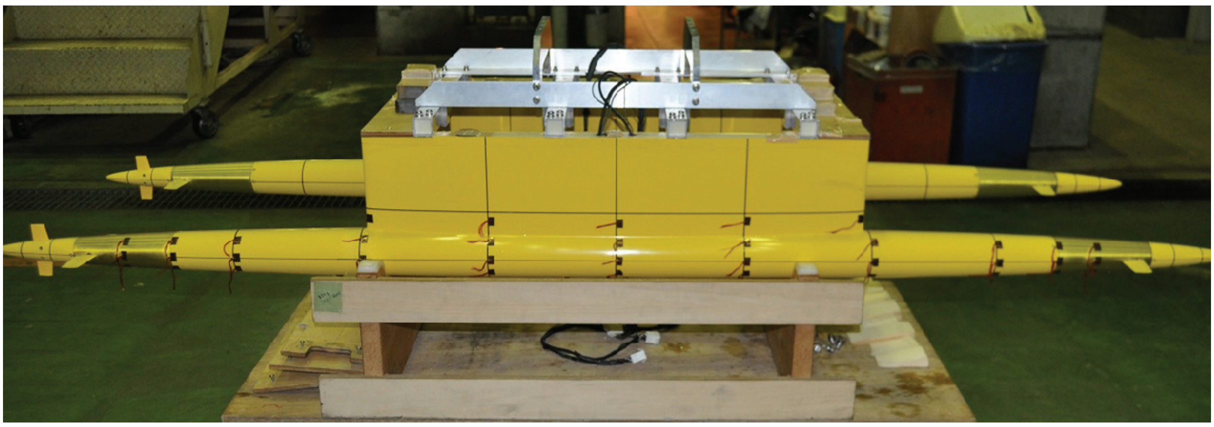

Figure 7: Small tufts attached to model for flow visualization test

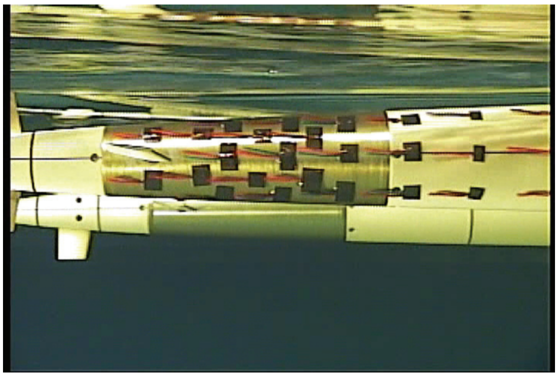

Attack angle of aft fin α_{c3} >0

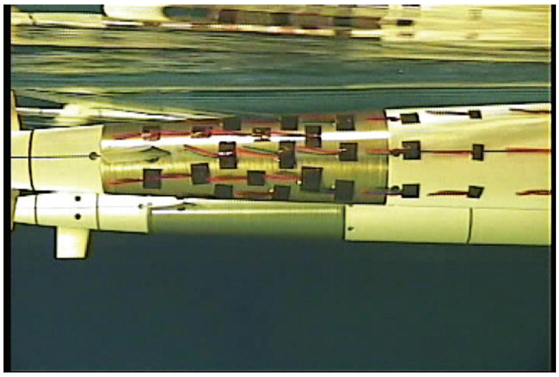

Attack angle of fin α_{c5} <0

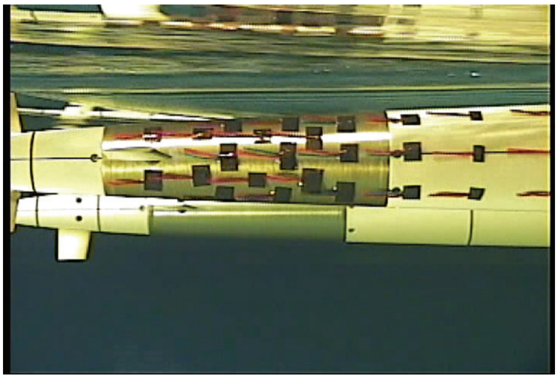

Attack angle of aft fin α_{c3} =0

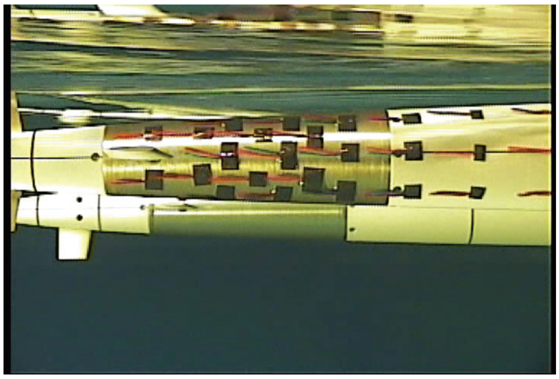

Attack angle of fin α_{c5} =0

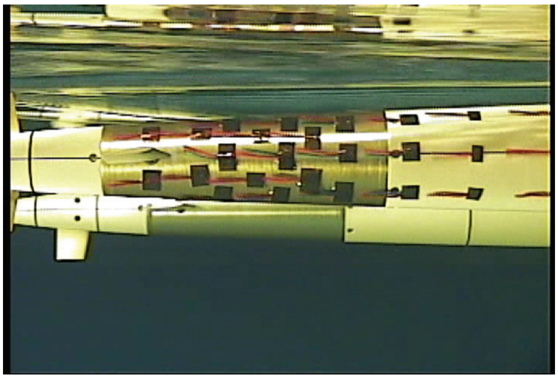

Attack angle of fin α_{c3} <0

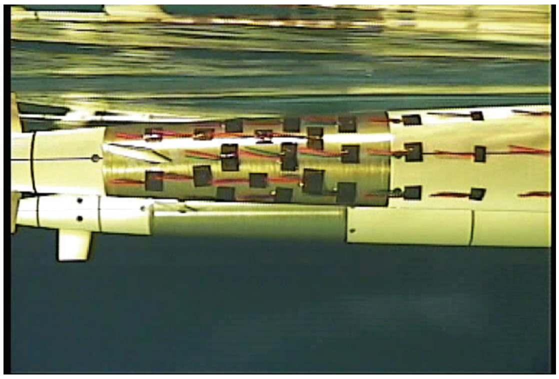

Attack angle of fin α_{c5} >0

(a) Heave control mode, ω =7.0 rad/s

(b) Pitch control mode, ω =11.1 rad/s

Figure 8: Visualization experiments to search the flow around aft fin

As the result, it is obtained that $k_{W(B)}$ or $k_{B(W)}$ is equal to 0.93 or 0.35, and $(C_{L\alpha})_{W(B)}$ or $(C_{L\alpha})_{B(W)}$ is equal to 2.27 or 0.85 respectively. Accordingly, the lift-curve slope $(C_{L\alpha})_{total}$ is equal to 3.12 1/rad calculated from Equation (37). Next, the calculated results by using 3D-RPM is discussed. As shown in Figure 6 (b), the value of $(C_{L\alpha})_W$ calculated in the case that the single fin rotates independently under the free surface is approximately equal to 2.73 1/rad. Also, the value of $k_{W(B)}$, $k_{B(W)}$, $(C_{L\alpha})_{W(B)}$ or $(C_{L\alpha})_{B(W)}$ is calculated as shown in Table 2. Consequently, $(C_{L\alpha})_{total}$ is equal to 3.21 in the heave control mode or 3.14 in the pitch control mode. On the other hand, the experimental value of $(C_{L\alpha})_{total}$ is approximately equal to 3.25 1/rad when the frequency gets close to the steady state i.e. ω=0 rad/s, especially in the case of the fore fins as shown in Figure 5 or Figure 6.

Table 2: Summary of body-fin interference on lift

	Aerodynamics Pitts et al.	3D-RPM		Experiment	
		heave	pitch	heave	pitch
$(C_{L\alpha})_W$	2.44	2.73			
$k_{W(B)}$	0.93	0.88	0.88		
$k_{B(W)}$	0.35	0.30	0.27		
$(C_{L\alpha})_{W(B)}$	2.27	2.39	2.39		
$(C_{L\alpha})_{B(W)}$	0.85	0.82	0.75		
$(C_{L\alpha})_{total}$	3.12	3.21	3.14	3.25	3.24

The estimated and experimental results of the lift-curve slope $C_{L\alpha}$ and the body-fin interference factors $k_{W(B)}$ and $k_{B(W)}$ are summarized in Table 2, where the numbers indicate the values of the steady state. Also the numbers calculated by means of 3-D RPM represent the values in the case of the fore fin except for the $(C_{L\alpha})_W$. From the table, it can be confirmed that estimation by means of aerodynamics theory works well too in the hydrodynamic problem. Also, the values of the $k_{W(B)}$, $k_{B(W)}$ and $C_{L\alpha}$ based on the aerodynamics, the 3-D RPM and the experimental measurement agree well with each other.

5. CONCLUSIONS

One of the important problems in determining the seaworthiness of the RFS in waves is the effect of the lift generated by the small underwater control fins on the ship motion responses, especially the negative influence of the unsteady characteristics of the lift on the magnitude of the control gains for ship motions.

In the present study, theoretical calculations using the frequency-domain 3D-Rankine Panel Method have been carried out to evaluate the unsteady lift characteristics. The time lag and the interference between the fore fin, the aft fin and the hull in the lift generation is taken into account in the calculations. Then, those results have been used in a comparative review with the experimental results.

Firstly, the calculations have been carried out for the condition that the wake sheet of the fore fin passes above the aft fin with a height of 25 mm based on the result of visualization experiments of the flow around the lower hull. The calculated results for the amplitude of the lift agree very well with the experimental results, while the calculated results for the phase lag demonstrate only the tendency of the experimental results.

Secondly, from the calculated and experimental results, it is observed that:

- The amplitude and the time lag i.e. the phase lag of the lift-curve slope for the aft fin have periodical humps and hollows with respect to the angular frequency in both the cases of heave and pitch control modes, while there exists no hump and hollow for that of the fore fin.
- In the case where only the fore fin is rotated and the aft fin is fixed at zero angle, the amplitude of the lift generated by the aft fin shows a value which is more than zero. This is principally caused by the influence of the wake sheet of the fore fin.
- Regarding the fin-hull interference factors $k_{W(B)}$ and $k_{B(W)}$ and lift-curve slope $C_{L\alpha}$ in the steady state, the values based on the aerodynamics, the 3-D RPM calculation and the experimental measurement agree well with each other. For example, the calculated result of the lift-curve slope is approximately equal to 3.2 1/rad. This is equivalent to the value predicted by the aerodynamic theory or to the value measured in the experiments in the model basin.

6. ACKNOWLEDGEMENTS

This study has been performed by the assist of grant-in-aid for scientific research (No. 23246151), Japan Society for the Promotion of Science.

7. REFERENCES

1. TAKARADA, N., TAKEZAWA, S., HIRAYAMA, T., WANG, X., KOBAYASHI, K. and SAKURAI, H., R&D of a displacement-type high speed ship (Part 4: Seakeeping qualities in high speed range), *Journal of the Society of Naval Architects of Japan*, *Volume 171*, *pp 73–82*, 1992.
2. PAPANIKOLAOU, A., ZARAPHONITIS, G. and ANDROULAKAKIS, M., Preliminary design of a high-speed SWATH passenger/car ferry, *Journal Marine Technology*, *SNAME*, *Volume 28*, *No. 3*, *pp 129–141*, 1991.
3. ARMSTRONG, T. and HOLDEN, K., A new generation of large fast ferry – from concept to contact reality, *7th International Conference on Fast Sea Transportation (FAST 2003)*, *pp 75–84*, 2003.
4. LEE, C. M., Theoretical prediction of motion of Small-Waterplane-Area, Twin-Hull (SWATH) ships in waves, *DTNSRDC Report*, *SPD–76–0046*, 1976.
5. LEE, C. M. and CURPHEY, M., Prediction of motion, stability, and wave load of Small-Waterplane-Area Twin-Hull Ships, *SNAME Transactions*, *Volume 85*, *9–4130*, 1977.
6. MATSUSHIMA, M., NAKAMURA, H. and KUNITAKE Y., Seakeeping of A Semi-Submerged Catamaran (SSC) Vessel, *Transactions of the West-Japan Society of Naval Architects*, *Volume 63*, *pp 97–114,* 1982.
7. NISHIYAMA, T., Unsteady hydrofoil theory, Part 1 Characteristics of hydrofoil moving at constant speed under sinusoidal waves, *Journal of the Society of Naval Architects of Japan*, *Volume 112*, *pp 1-14*, 1962.
8. NISHIYAMA, T., Unsteady hydrofoil theory, Part 2 Characteristics of hydrofoil performing heave and pitch while moving at constant forward speed in still water, *Journal of the Society of Naval Architects of Japan*, *Volume 112*, *pp 14-19*, 1962.
9. KYOZUKA, Y., HORI, T. and KOTERAYAMA, W., Unsteady Hydrodynamic Forces on a Lifting Body (Second Report, Interaction of Lift between Body and Wing), *Journal of the Society of Naval Architects of Japan*, *Volume 168*, *pp 243–251*, 1990.
10. KINOSHITA, T. and KOBAYASHI, H., Improving rower motion and rowing equipment

by using rowing velocity prediction program with estimating hydrodynamic load acting on an oar blade, *Transactions of RINA*, *Volume 146*, *Part B2*, *International Journal of Small Craft Technology*, *pp 16–26*, 2004.

11. YOSHIDA, T., FUJITA, Y. and FUJINO, M., A proposal of the CS-Swath as a Transocean High Speed Ship, *Transactions of RINA*, *Volume 142 (B)*, *pp 136–149*, 2000.
12. YOSHIDA, M., KIHARA, H., IWASHITA, H., KANDA, M. and KINOSHITA, T., Superior seaworthiness of a Resonance-Free fast oceangoing SWATH, *Transactions of RINA*, *Volume 156*, *Part A4*, *International Journal of Maritime Engineering*, *pp A-315–A-332*, 2014.
13. ELANGOVAN, M., IWASHITA, H., SAITO, H. and ITO, A., Seakeeping Estimations of Fast Ships with Transom Stern, *Journal of the Japan Society of Naval Architects and Ocean Engineers*, *Volume 7*, *pp 195–206*, 2008.
14. IWASHITA, H., HIDAKA, Y., SUENAGA, M. and SHIBATA, H., A study on the hydrodynamic interaction between submerged lifting and non-lifting bodies advancing in waves, *Journal of the Society of Naval Architects of Japan*, *Volume 192*, *pp 209–218*, 2002.
15. MORINO, L. and KUO, C. C., Subsonic potential aerodynamics for complex configurations: A general theory, *AIAA Journal*, *Volume 12*, *No. 2*, *pp 191–197*, 1974.
16. SCLAVOUNOS, P. D. and NAKOS, D. E., Stability analysis of panel method for free-surface flow with forward speed, *17th Symposium on Naval Hydrodynamics*, *The Hague*, 1988.
17. YOSHIDA, M., KIHARA, H., IWASHITA, H. and KINOSHITA, T., Motion control of Resonance-Free SWATH using small movable fins, *The second international conference on high speed marine vessels (IHSMV 2011)*, *RINA*, 2011.
18. YOSHIDA, M., IWASHITA, H., KIHARA, H. and KINOSHITA, T., Seaworthiness of Resonance-Free SWATH as an oceangoing fast ship, *9th Symposium on high speed marine vehicles (HSMV 2011)*, 2011.
19. PITTS, W. C., NIELSEN, J. N. and KAATTARI, G. E., Lift and center of pressure of wing-body-tail combinations at subsonic, transonic, and supersonic speeds, *National Advisory Committee for Aeronautics*, *Report 1307*, 1959.
20. WHICKER, L. F. and FAHLNER, L. F., Free-Stream Characteristics of a Family of Low-Aspect-Ratio, All-Movable Control Surfaces for Application to Ship Design, *David Taylor Model Basin Report 933*, 1958.